Letter

Pressure-induced superconductivity in the topological crystalline insulator NaCd$_4$As$_3$

Haiyang Yang [1,2,3] Yonghui Zhou [1,2,*] Jing Wang,[1,2] Shuyang Wang,[1,2] Chao An,[4] Ying Zhou,[4] Xuliang Chen,[1,2] Lili Zhang [5] Xiaoping Yang [1,2,†] and Zhaorong Yang [1,2,4,6,‡]

[1]*Anhui Key Laboratory of Low-Energy Quantum Materials and Devices,*
High Magnetic Field Laboratory, HFIPS, Chinese Academy of Sciences, Hefei 230031, China
[2]*Science Island Branch of Graduate School, University of Science and Technology of China, Hefei 230026, China*
[3]*Institute of Advanced Magnetic Materials, College of Materials and Environmental Engineering,*
Hangzhou Dianzi University, Hangzhou 310012, China
[4]*Institutes of Physical Science and Information Technology, Anhui University, Hefei 230601, China*
[5]*Shanghai Synchrotron Radiation Facility, Shanghai Advanced Research Institute, Chinese Academy of Sciences, Shanghai 201204, China*
[6]*Collaborative Innovation Center of Advanced Microstructures, Nanjing University, Nanjing 210093, China*

Recently, a united symmetry-protected topological crystalline insulator (TCI) NaCd$_4$As$_3$ has been discovered experimentally, which further features a temperature-driven transformation from TCI to TI due to the mirror symmetry broken across a rhombohedral-to-monoclinic structural transition. Here, we report the pressure tuning of structural property and emergence of superconductivity in TCI NaCd$_4$As$_3$ by comprehensive high-pressure experiments in diamond-anvil cell. Temperature-dependent Raman measurements show that the structural transition temperature gradually reduces upon compression and is completely suppressed above ~ 4 GPa. The stable rhombohedral phase further undergoes amorphization evidenced by synchrotron x-ray-diffraction result, which sets in at 20.7 GPa and completes at 34.4 GPa. Along with the complete amorphization, the metallization and superconductivity with a critical temperature $T_c \sim 2.5$ K appear simultaneously, as observed in transport experiments. We argue that the sudden enhancement in T_c across 60.0 GPa is likely related to the pressure-driven amorphous polymorphism. Our finding unravels the fundamental structure-property relationship and highly tunable crystallographic symmetry in NaCd$_4$As$_3$ by external pressure, potentially sparking further investigations via alternative tuning strategies.

Symmetry-protected topological quantum states have attracted wide and intensive investigations since the discovery of topological insulators (TIs) [1–3]. The well-known TIs host an odd number of surface Dirac cones protected by time-reversal symmetry. By contrast, in other topological materials the topological band structures can couple with the special symmetry, thus creating distinct physical properties. For example, topological crystalline insulators (TCIs) possess an even number of surface Dirac cones, which are protected by the combination of time-reversal symmetry and mirror (rotation) symmetry and are robust against magnetic dopants or impurities [4–6]. In addition, it has been shown that when topological materials fall into superconducting state, topological superconductivity characterized by exotic Majorana fermions may be realized [7].

Recently, ternary TCI NaCd$_4$As$_3$ protected by the time-reversal and mirror symmetry has been verified by the theoretical and angle-resolved photoemission spectroscopy studies [8–12]. Namely, NaCd$_4$As$_3$ features one mirror symmetry-protected Dirac cone at T point of the surface Brillouin zone and one time-reversal symmetry-protected band inversion at the Γ point. Interestingly, upon cooling the electronic state of NaCd$_4$As$_3$ transforms from TCI to TI, which is induced by the disruption of mirror symmetry due to a rhombohedral-to-monoclinic structural transition [12,13]. Thus, the natural incorporation of TCI and TI in temperature-dependent NaCd$_4$As$_3$ provides a unique platform for investigating the intrinsic correlation between structure, electronic properties, and underlying nontrivial topology.

Pressure, as one of the fundamental thermodynamic parameters, serves as an effective and clean approach to tune the crystallographic symmetry and electronic states, which has been widely employed in topological electronic materials [14–21]. In this work, we performed comprehensive Raman spectroscopy, x-ray diffraction (XRD), and electrical transport measurements to elucidate the relationship between structural and electronic properties of TCI NaCd$_4$As$_3$ via applying external pressure. We show that the rhombohedral-to-monoclinic transition temperature gradually reduces upon compression and is completely suppressed above ~ 4 GPa. Further increase in pressure leads to the occurrence of amorphization between 20.7 and 34.4 GPa. Along with the complete amorphization, we observe the concurrence of metallization and superconductivity. We also unravel the presence of anomalous superconductivity evolution versus
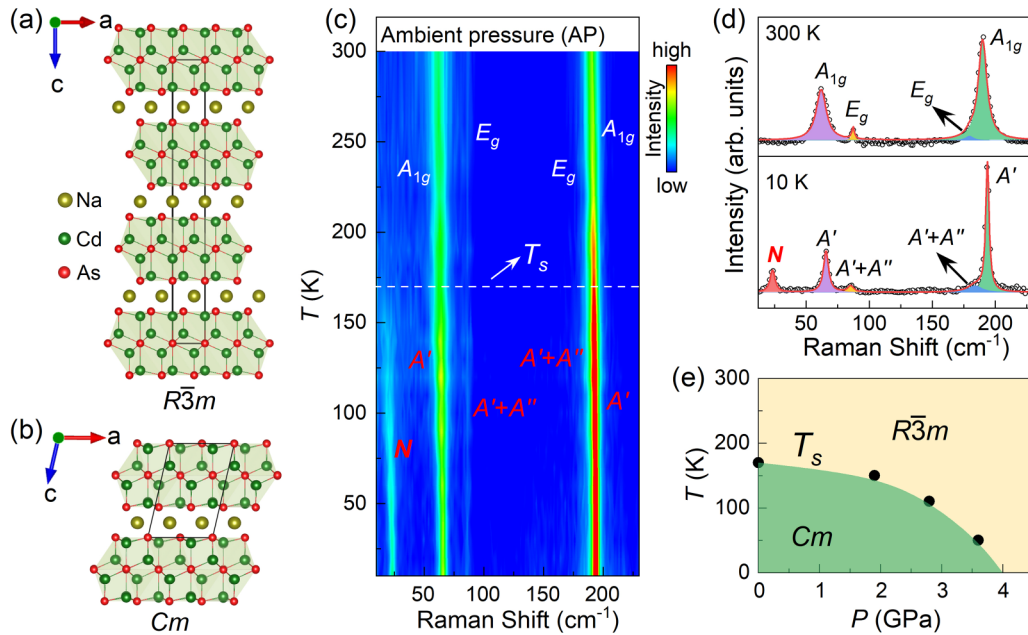

FIG. 1. Schematic crystal structures of NaCd$_4$As$_3$: (a) rhombohedral $R\bar{3}m$ phase at room temperature and (b) monoclinic Cm phase at low temperature. The Na, Cd, and As atoms are depicted as chartreuse, green, and red spheres, respectively. (c) Contour plot of Raman spectra at various temperatures under ambient pressure (AP). (d) Raman spectrum of NaCd$_4$As$_3$ single crystal at 300 and 10 K. The solid red line represents the fitting of Raman spectra by using Lorentzian function. (e) Pressure evolution of crystal structure of NaCd$_4$As$_3$. The T_s denotes the temperature of structural phase transition from $R\bar{3}m$ phase to Cm phase.

pressure, which could be related to the pressure-driven amorphous polymorphism.

Detailed experimental and computational methods and the supporting data are available in Supplemental Material [22] and Refs. [23–33]. NaCd$_4$As$_3$ crystallizes in a rhombohedral structure (space group $R\bar{3}m$, No. 166) at ambient condition. With decreasing temperature, NaCd$_4$As$_3$ becomes a monoclinic phase (space group Cm, No. 8) [12,13]. In both phases, the primary structural motifs consist of Cd-As layers intercalated by Na atom layers, as illustrated in Figs. 1(a) and 1(b). The rhombohedral-to-monoclinic structural transition is also reflected by our temperature-dependent Raman spectroscopy measurements. Figure 1(c) shows the temperature evolution of Raman spectra of NaCd$_4$As$_3$ at ambient pressure. Group theoretical analysis indicates that the rhombohedral structure possesses the point group D_{3d}, and its irreducible representation of Raman-active modes is given by $\Gamma = 3A_{1g} + 3E_g$ (Table S1). As shown in Fig. 1(d), four Raman-active modes are observed in the range of $10 - 230\,\text{cm}^{-1}$ at 300 K, including the A_{1g}, E_g, E_g, and A_{1g} modes at 61.8, 87.1, 179.4, and 189.8 cm^{-1}, respectively. The A_{1g} mode involves interlayer vibrations of Cd-As layers along the c axis, while the doubly degenerate E_g modes correspond to the vibrations of Cd and As atoms in the ab plane (Fig. S1). Upon cooling temperature to 170 K, a Raman peak N emerges at 18.3 cm^{-1}. According to the group-symmetry analysis (Table S2), the observed Raman modes in low-temperature monoclinic phase are derived from A_{1g} or E_g mode, except for the N mode, as shown in Fig. S1. Thus, the appearance of the N peak can be viewed as a fingerprint, signaling the structural transition in NaCd$_4$As$_3$. After applying external pressure, the pressure evolution of the structural transition temperature (T_s) was further explored

by the temperature-dependent Raman experiment (Fig. S2). At 1.9 GPa, the low-frequency mode N appears at $\sim$ 150 K, which indicates the lower T_s compared to that of ambient pressure. As pressure increases, the T_s gradually decreases and is completely suppressed above $\sim$ 4 GPa, suggesting that the rhombohedral phase becomes the stable high-pressure phase, as depicted in Fig. 1(e).

To further study the evolution of high-pressure rhombohedral NaCd$_4$As$_3$ at higher pressures, we conducted *in situ* synchrotron XRD experiment at room temperature. Figure 2(a) presents the representative XRD patterns at various pressures up to 71.4 GPa under compression and decompression. At 0.5 GPa, the pattern can be indexed with the rhombohedral $R\bar{3}m$ phase of NaCd$_4$As$_3$, except three peaks from a rhenium gasket (marked by asterisks) [Fig. 2(b)]. As the pressure increases, the diffraction peaks shift toward higher angles due to lattice compression. At 20.7 GPa, all the peak intensity suddenly reduces, leaving only a subset of peaks and a broad hump near 15° [Fig. 2(c)]. This indicates the onset of amorphization under pressure. Further compression to 34.4 GPa leads to a complete amorphization, reflected by the disappearance of peaks from pristine crystalline NaCd$_4$As$_3$. Upon further compression, this broad hump becomes more and more pronounced, while no new peaks from sample are discernible even at the highest pressure of 71.4 GPa. For crystalline NaCd$_4$As$_3$, the lattice parameters a, c, and volume V were extracted through fitting, as plotted in Figs. 2(d) and 2(e). The pressure-dependent volume can be well fitted by using the third-order Birch-Murnaghan equation of state [34], yielding the ambient pressure volume $V_0 = 569.5 \pm 5.6\,\text{Å}^3$, the bulk modulus $B_0 = 37.7 \pm 2.9\,\text{GPa}$, and its first-order derivative of the bulk modulus at ambient
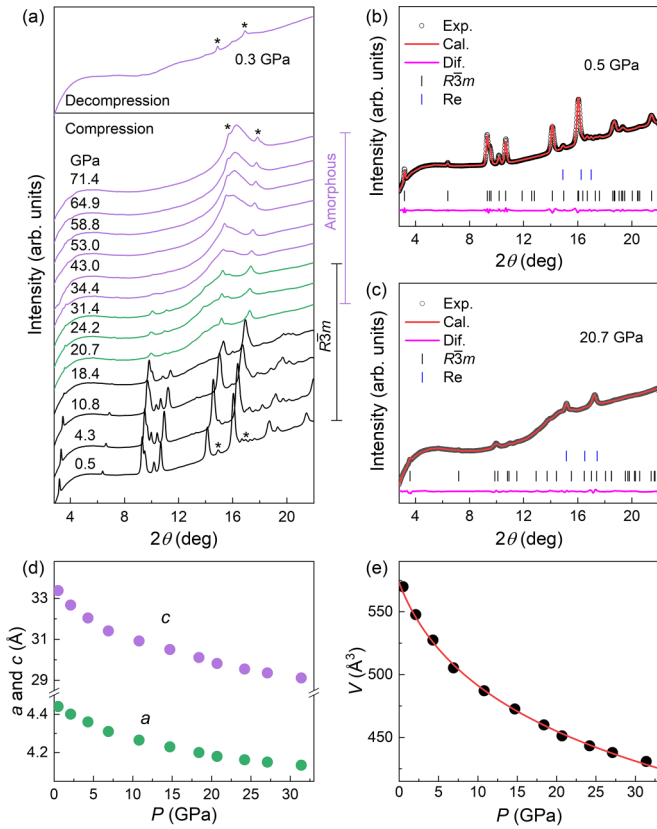
FIG. 2. (a) Pressure evolution of XRD pattern of NaCd$_4$As$_3$ at room temperature. The asterisks (*) denote the diffraction peaks for the rhenium gasket. (b), (c) Typical fitting results at 0.5 and 20.7 GPa by the Le Bail method. (d) Lattice parameters a and c as a function of pressure. (e) Volume as a function of pressure. The solid red line denotes the fitting for the pristine rhombohedral phase according to the third-order Birch-Murnaghan equation of states.
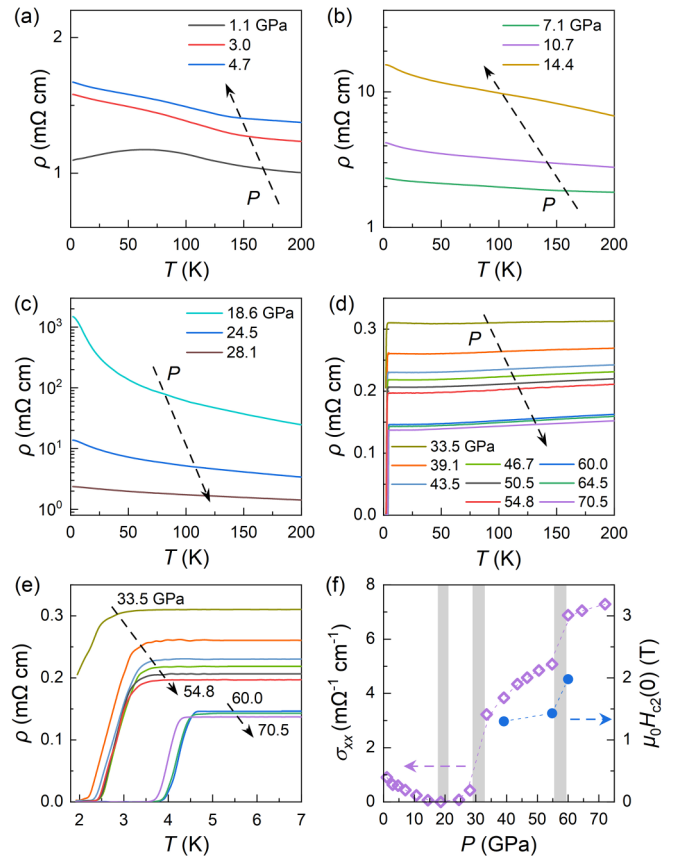

FIG. 3. (a)–(d) Temperature dependence of resistivity curves of NaCd$_4$As$_3$ from 1.1 to 70.5 GPa. (e) A zoomed-in view of the $\rho(T)$ curves near the superconducting transition temperature. (f) Left: the electrical conductivity at 10 K as a function of pressure. Right: the superconducting upper critical field versus pressure.

pressure $B_0' = 8.4 \pm 0.4$, respectively. When the pressure is released to 0.3 GPa, the XRD pattern only exhibits two peaks from the rhenium gasket, indicating the irreversibility of the amorphization after a compression-decompression cycle.

Next, we performed high-pressure electrical transport measurements to explore the electronic properties according to the structural evolution of NaCd$_4$As$_3$. At ambient pressure, NaCd$_4$As$_3$ displays metallic behavior [Fig. S3(c)], which can be related to the contribution of conduction-band electrons near the Fermi level [12]. After applying external pressure, the temperature-dependent resistivity $\rho(T)$ curve shows a semi-conducting behavior at 4.7 GPa in the whole temperature range [Fig. 3(a)]. A possible reason for the semiconducting behavior under pressure is the suppression of mobility while carrier density changes little [35,36], as shown in Fig. S4(b). Above 18.6 GPa, the resistivity over the whole temperature range begins to decrease rapidly [Fig. 3(c)]. Upon compression to 33.5 GPa, the pressure-induced metallic conductivity appears, accompanied by a resistivity drop around 2.5 K [Fig. 3(d)]. At 39.1 GPa, zero resistivity is observed, indicating the presence of superconductivity [Fig. 3(e)]. The superconducting transition temperature T_c is defined by the resistivity criterion of $\rho_{cri} = 90\%\rho_n$ (ρ_n is the normal-state resistivity). As seen in Fig. 3(e), the T_c remains nearly con-

stant around 3.2 K between 39.1 and 54.8 GPa, and steeply increases to 4.5 K at 60.0 GPa and above.

We then measured $\rho(T)$ curves under various magnetic fields along the c axis. As shown in Fig. S5 [22], superconductivity is gradually suppressed with increasing magnetic field. Because amorphous superconductors can have strong electron-phonon coupling [37], we estimated the zero-temperature upper critical field $\mu_0 H_{c2}(0)$ value for each pressure by a simple linear extrapolation, yielding $\mu_0 H_{c2}(0)$ of 1.30 T at 39.1 GPa, 1.43 T at 54.8 GPa, and 1.98 T at 60.0 GPa, respectively. These values are smaller than the Pauli paramagnetic limit of 1.84 T_c, indicating absence of Pauli pair breaking. Figure 3(f) summarizes the effect of pressure on the electrical conductivity and upper critical field of NaCd$_4$As$_3$, revealing three abnormal pressure points of 20.7, 34.4, and 60.0 GPa. The first two anomalies are associated with the amorphization process. We further analyzed the low-temperature $\rho(T)$ curves using a power law of $\rho(T) = \rho_0 + AT^n$. The extracted exponent n and the temperature prefactor A as a function of pressure are displayed in Fig. S6. It can be seen that the value of n decreases from ~ 4.5 to ~ 3 across 60 GPa, suggesting a possible variation of electron-phonon scattering mechanism [38,39]. In addition to the consistent anomaly in transport properties, such as the abrupt increase in superconducting temperature T_c, the superconducting up-
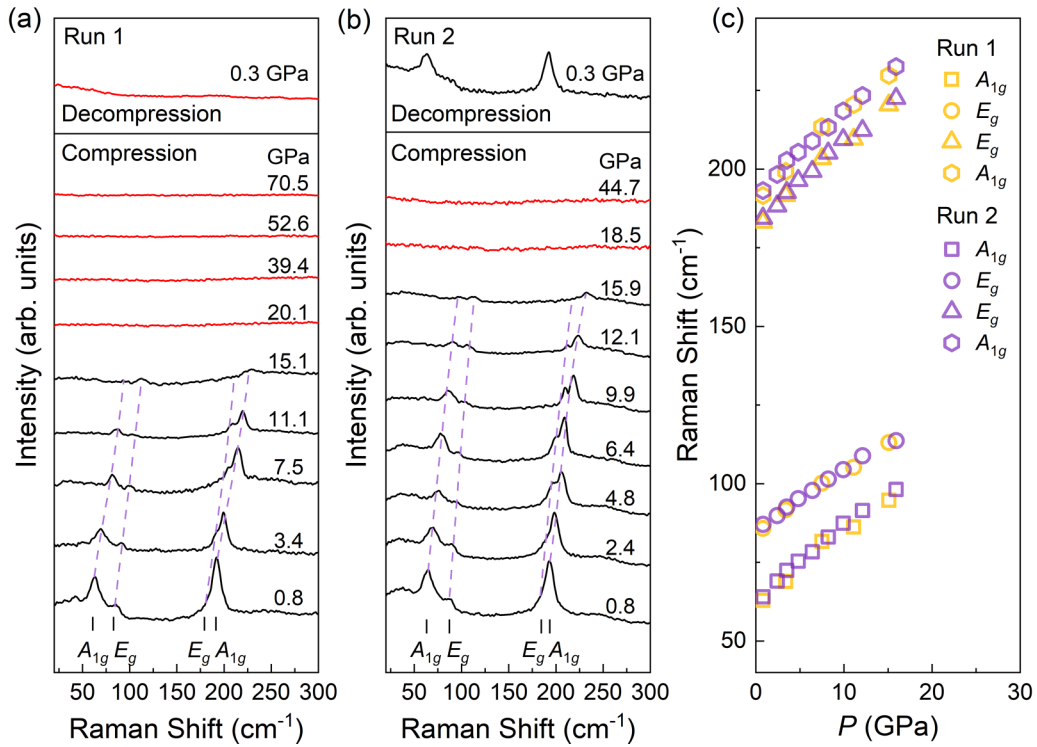
FIG. 4. (a), (b) show the room-temperature Raman spectra of $NaCd_4As_3$ single crystal under various pressures: from 0.8 to 70.5 GPa in run 1 and from 0.8 to 44.7 GPa in run 2, respectively. The vertical solid lines represent the peak positions. The dashed lines are guides to the eye. (c) Pressure dependence of Raman frequencies in $NaCd_4As_3$.

per critical magnetic field, and the normal-state conductivity around 60 GPa, we suggest two superconducting phases may embed in amorphous $NaCd_4As_3$.

To explore the possible phase transition within amorphous $NaCd_4As_3$ under higher pressure, we further performed comparative experiments using room-temperature Raman spectroscopy, as shown in Fig. 4. In run 1, we gradually increased pressure from 0.8 to 70.5 GPa, with similar maximum pressure in XRD experiment. As shown in Fig. 4(a), all the Raman modes exhibit blueshift versus pressure and become featureless at 20.1 GPa and above. This phenomenon should be related to the occurrence of amorphization evidenced by our XRD result. After releasing pressure from 70.5 to 0.3 GPa, we note that the original Raman modes do not recover, in line with the irreversibility of XRD experiments [Fig. 2(a)]. By contrast, when we apply the pressure to 44.7 GPa and then release the pressure to 0.3 GPa, the Raman spectrum initially becomes featureless and then returns to its pristine state [Fig. 4(b)]. This discrepancy in these two decompression processes strongly suggests an essential change within the frame of amorphous structure between 44.7 and 70.5 GPa. This phenomenon is reminiscent of the pressure-driven amorphous polymorphism, such as Bi [37], Ge [40], and Sb_2Se_3 [41]. It can be responsible for the abrupt enhancement of electrical conductivity, as well as the superconducting upper critical field and T_c around 60.0 GPa [Figs. 3(e) and 3(f)].

While it is common to observe superconductivity in an amorphous phase [37], our study revealed that in high-pressure amorphous $NaCd_4As_3$, superconductivity not only emerges at 33.5 GPa but also is significantly enhanced at ~ 60.0 GPa due to the occurrence of amorphous

polymorphism, as evidenced by the XRD and Raman results. By combining the pressure evolution of the structure and transport properties, we constructed a temperature-pressure phase diagram to elucidate the structure-property relationship in pressurized $NaCd_4As_3$, as shown in Fig. 5. It indicates vividly a structural origin of the unusual evolution of electronic properties. First, the low-temperature monoclinic *Cm* phase gradually suppresses upon compression. Above ~ 4 GPa, the rhombohedral phase becomes predominant. Second, when approaching a critical pressure of $P_{c1} \sim 20.7$ GPa, the rhombohedral phase partially transforms into an amorphous phase. Due to the occurrence of amorphization, the electrical conductivity is slightly enhanced. When the amorphization process completes at $P_{c2} \sim 34.4$ GPa, the electrical conductivity gets steeply enhanced, which is accompanied by the concurrence of metallization and superconductivity with a $T_c \sim 2.5$ K. Last, upon further compression to 60.0 GPa, the conductivity of $NaCd_4As_3$ is further enhanced and T_c is significantly increased to 4.5 K. Considering the presence of pressure-driven amorphous polymorphism evidenced from the XRD and Raman results, the anomalies in transport properties can be accounted for, including the sudden enhancement of electrical conductivity, the superconducting upper critical field, and T_c around 60.0 GPa. On the other hand, we note that the room-temperature rhombohedral phase is TCI and persists to P_{c1}. Whether the TCI-to-TI transition is strongly coupled to the structural transition under external pressure needs further investigation in the future.

In summary, we have systematically investigated the effect of pressure on the crystal structure and electrical transport properties of TCI $NaCd_4As_3$. We show that pressure-tuned
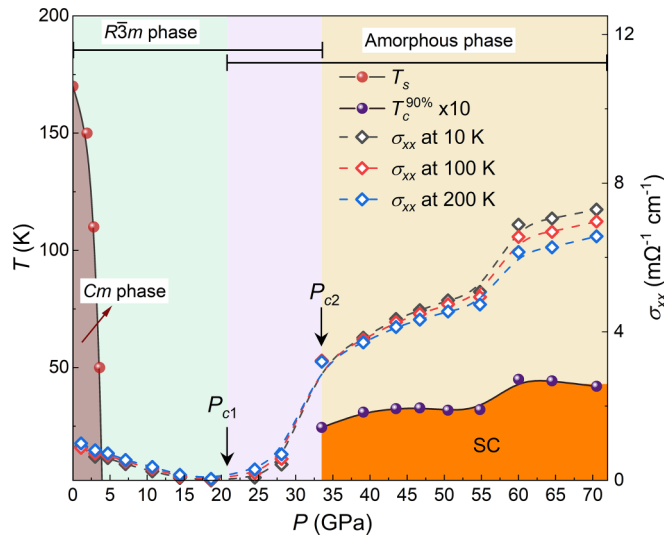
FIG. 5. Pressure evolution of the structural and electronic properties of $NaCd_4As_3$. The colored areas are guides to the eye, indicating three distinct structural phases: $R\bar{3}m$ phase, Cm phase, and amorphous phase. The black arrow indicates the critical pressure P_{c1}, coinciding with the onset of the $R\bar{3}m$ phase to amorphous phase. The critical pressure P_{c2} denotes the complete disappearance of the crystalline phase and onset of superconductivity.

electronic properties correlate with the structural evolution versus pressure. Upon compression, the room-temperature rhombohedral phase persists to the base temperature

above ~ 4 GPa. Starting from 20.7 GPa, the rhombohedral phase becomes unstable and displays partial amorphization. The metallization and superconductivity appear simultaneously when the amorphization process completes at 34.4 GPa. With further increasing pressure, the superconducting T_c remains nearly constant and undergoes a sudden enhancement around 60.0 GPa, which is likely related to the pressure-driven amorphous polymorphism. These findings offer a deep understanding of the structure-property relationship in pressurized $NaCd_4As_3$.

[1] M. Z. Hasan and C. L. Kane, Colloquium: Topological insulators, Rev. Mod. Phys. **82**, 3045 (2010).

[2] C. K. Chiu, J. C. Y. Teo, A. P. Schnyder, and S. Ryu, Classification of topological quantum matter with symmetries, Rev. Mod. Phys. **88**, 035005 (2016).

[3] X. G. Wen, Colloquium: Zoo of quantum-topological phases of matter, Rev. Mod. Phys. **89**, 041004 (2017).

[4] L. Fu, Topological crystalline insulators, Phys. Rev. Lett. **106**, 106802 (2011).

[5] Y. Ando and L. Fu, Topological crystalline insulators and topological superconductors: From concepts to materials, Annu. Rev. Condens. Matter Phys. **6**, 361 (2015).

[6] T. Neupert and F. Schindler, Topological crystalline insulators, in *Topological Matter: Lectures from the Topological Matter School 2017*, edited by D. Bercioux, J. Cayssol, M. G. Vergniory, and M. Reyes Calvo (Springer International, Cham, 2018), pp. 31–61.

[7] X. L. Qi and S. C. Zhang, Topological insulators and superconductors, Rev. Mod. Phys. **83**, 1057 (2011).

[8] T. T. Zhang, Y. Jiang, Z. D. Song, H. Huang, Y. Q. He, Z. Fang, H. M. Weng, and C. Fang, Catalogue of topological electronic materials, Nature (London) **566**, 475 (2019).

[9] M. G. Vergniory, L. Elcoro, C. Felser, N. Regnault, B. A. Bernevig, and Z. J. Wang, A complete catalogue of high-quality topological materials, Nature (London) **566**, 480 (2019).

[10] F. Tang, H. C. Po, A. Vishwanath, and X. G. Wan, Comprehensive search for topological materials using symmetry indicators, Nature (London) **566**, 486 (2019).

[11] F. Tang and X. G. Wan, Effective models for nearly ideal Dirac semimetals, Front. Phys. **14**, 43603 (2019).

[12] Y.-Y. Wang, C. Zhong, M. Li, W.-L. Zhu, W.-J. Hou, W.-H. Song, Q.-X. Dong, Y.-F. Huang, S. Zhang, Z.-A. Ren, S. Wang, and G.-F. Chen, Magnetotransport properties and topological phase transition in $NaCd_4As_3$, Phys. Rev. B **102**, 115122 (2020).

[13] C. Grotz, M. Baumgartner, K. M. Freitag, F. Baumer, and T. Nilges, Polymorphism in Zintl phases ACd_4Pn_3: Modulated structures of $NaCd_4Pn_3$ with Pn = P, As, Inorg. Chem **55**, 7764 (2016).

[14] K. Kirshenbaum, P. S. Syers, A. P. Hope, N. P. Butch, J. R. Jeffries, S. T. Weir, J. J. Hamlin, M. B. Maple, Y. K. Vohra, and J. Paglione, Pressure-induced unconventional superconducting phase in the topological insulator Bi_2Se_3, Phys. Rev. Lett. **111**, 087001 (2013).

[15] Y. H. Zhou, J. F. Wu, W. Ning, N. N. Li, Y. P. Du, X. L. Chen, R. R. Zhang, Z. H. Chi, X. F. Wang, X. D. Zhu, P. C. Lu, C. Ji, X. G. Wan, Z. R. Yang, J. Sun, W. G. Yang, M. L. Tian, Y. H. Zhang, and H. K. Mao, Pressure-induced superconductivity in a three-dimensional topological material $ZrTe_5$, Proc. Natl. Acad. Sci. USA **113**, 2904 (2016).

[16] J. L. Zhang, C. Y. Guo, X. D. Zhu, L. Ma, G. L. Zheng, Y. Q. Wang, L. Pi, Y. Chen, H. Q. Yuan, and M. L. Tian, Disruption of the accidental Dirac semimetal state in ZrTe$_5$ under hydrostatic pressure, Phys. Rev. Lett. **118**, 206601 (2017).

[17] Y. P. Qi, W. J. Shi, P. G. Naumov, N. Kumar, R. Sankar, W. Schnelle, C. Shekhar, F. C. Chou, C. Felser, B. H. Yan, and S. A. Medvedev, Topological quantum phase transition and superconductivity induced by pressure in the bismuth tellurohalide BiTeI, Adv. Mater. **29**, 1605965 (2017).

[18] X. Li, D. Y. Chen, M. L. Jin, D. S. Ma, Y. F. Ge, J. P. Sun, W. H. Guo, H. Sun, J. F. Han, W. D. Xiao, J. X. Duan, Q. S. Wang, C. C. Liu, R. Q. Zou, J. G. Cheng, C. Q. Jin, J. S. Zhou, J. B. Goodenough, J. L. Zhu, and Y. G. Yao, Pressure-induced phase transitions and superconductivity in a quasi-1-dimensional topological crystalline insulator $\alpha-$Bi$_4$Br$_4$, Proc. Natl. Acad. Sci. USA **116**, 17696 (2019).

[19] C. Y. Pei, P. H. Huang, P. Zhu, L. L. Liu, Q. Wang, Y. Zhao, L. L. Gao, C. H. Li, W. Z. Cao, J. Lv, X. Li, Z. W. Wang, Y. G. Yao, B. H. Yan, C. Felser, Y. L. Chen, H. Y. Liu, and Y. P. Qi, Pressure-induced superconductivity extending across the topological phase transition in thallium-based topological materials, Cell Rep. Phys. Sci. **3**, 101094 (2022).

[20] T. Murtaza, H. Y. Yang, J. J. Feng, Y. Shen, Y. Ge, Y. Liu, C. Xu, W. Jiao, Y. Lv, C. J. Ridley, C. L. Bull, P. K. Biswas, R. Sankar, W. Zhou, B. Qian, X. Jiang, Z. Feng, Y. Zhou, Z. Zhu, Z. Yang, and X. Xu, Cascade of pressure-driven phase transitions in the topological nodal-line superconductor PbTaSe$_2$, Phys. Rev. B **106**, L060501 (2022).

[21] H. Y. Yang, Y. H. Zhou, S. Y. Wang, J. Wang, X. L. Chen, L. L. Zhang, C. C. Xu, and Z. R. Yang, Pressure-induced nontrivial Z_2 band topology and superconductivity in the transition metal chalcogenide Ta$_2$Ni$_3$Te$_5$, Phys. Rev. B **107**, L020503 (2023).

[22] See Supplemental Material at http://link.aps.org/supplemental/10.1103/PhysRevB.110.L060509 for the experimental and theoretical methods and other supporting data under pressure.

[23] H. Y. Yang, Y. H. Zhou, L. Y. Li, Z. Chen, Z. Y. Zhang, S. Y. Wang, J. Wang, X. L. Chen, C. An, Y. Zhou, M. Zhang, R. R. Zhang, X. D. Zhu, L. L. Zhang, X. P. Yang, and Z. R. Yang, Pressure-induced superconductivity in quasi-one-dimensional semimetal Ta$_2$PdSe$_6$, Phys. Rev. Mater. **6**, 084803 (2022).

[24] C. Prescher and V. B. Prakapenka, DIOPTAS: A program for reduction of two-dimensional X-ray diffraction data and data exploration, High Press. Res. **35**, 223 (2015).

[25] B. A. Hunter, *Rietica-A Visual Rietveld Program*. No. 20 (Summer, 1998), http://www.rietica.org: International Union

of Crystallography Commission on Powder Diffraction Newsletter.

[26] H. K. Mao, J. Xu, and P. M. Bell, Calibration of the ruby pressure gauge to 800 kbar under quasi-hydrostatic conditions, J. Geophys. Res. **91**, 4673 (1986).

[27] A. Togo and I. Tanaka, First principles phonon calculations in materials science, Scr. Mater. **108**, 1 (2015).

[28] G. Kresse and J. Hafner, *Ab initio* molecular dynamics for liquid metals, Phys. Rev. B **47**, 558 (1993).

[29] G. Kresse and J. Furthmüller, Efficient iterative schemes for ab initio total-energy calculations using a plane-wave basis set, Phys. Rev. B **54**, 11169 (1996).

[30] J. P. Perdew, K. Burke, and M. Ernzerhof, Generalized gradient approximation made simple, Phys. Rev. Lett. **77**, 3865 (1996).

[31] P. E. Blöchl, Projector augmented-wave method, Phys. Rev. B **50**, 17953 (1994).

[32] G. Kresse and D. Joubert, From ultrasoft pseudopotentials to the projector augmented-wave method, Phys. Rev. B **59**, 1758 (1999).

[33] F. Tran and P. Blaha, Accurate band gaps of semiconductors and insulators with a semilocal exchange-correlation potential, Phys. Rev. Lett. **102**, 226401 (2009).

[34] F. Birch, Finite elastic strain of cubic crystals, Phys. Rev. **71**, 809 (1947).

[35] J. J. Hamlin, J. R. Jeffries, N. P. Butch, P. Syers, D. A. Zocco, S. T. Weir, Y. K. Vohra, J. Paglione, and M. B. Maple, High pressure transport properties of the topological insulator Bi$_2$Se$_3$, J. Phys.: Condens. Matter **24**, 035602 (2012).

[36] Y. Zhou, P. Lu, Y. Du, X. Zhu, G. Zhang, R. Zhang, D. Shao, X. Chen, X. Wang, M. Tian, J. Sun, X. Wan, Z. Yang, W. Yang, Y. Zhang, and D. Xing, Pressure-induced new topological Weyl semimetal phase in TaAs, Phys. Rev. Lett. **117**, 146402 (2016).

[37] G. Bergmann, Amorphous metals and their superconductivity, Phys. Rep. **27**, 159 (1976).

[38] F. Nava, E. Mazzega, M. Michelini, O. Laborde, O. Thomas, J. P. Senateur, and R. Madar, Analysis of the electrical resistivity of Ti, Mo, Ta, and W monocrystalline disilicides, J. Appl. Phys. **65**, 1584 (1989).

[39] J. M. Ziman, *Electrons and Phonons: The Theory of Transport Phenomena in Solids* (Clarendon, Oxford, 1960).

[40] O. I. Barkalov, V. G. Tissen, P. F. McMillan, M. Wilson, A. Sella, and M. V. Nefedova, Pressure-induced transformations and superconductivity of amorphous germanium, Phys. Rev. B **82**, 020507(R) (2010).

[41] K. Zhang, M. Xu, N. Li, M. Xu, Q. Zhang, E. Greenberg, V. B. Prakapenka, Y. S. Chen, M. Wuttig, H. K. Mao, and W. Yang, Superconducting phase induced by a local structure transition in amorphous Sb$_2$Se$_3$ under high pressure, Phys. Rev. Lett. **127**, 127002 (2021).